Long-term deterioration of lubricant-infused nanoporous anodic aluminium oxide surface immersed in NaCl solution

Wu, Dequan; Ma, Lingwei; Liu, Bei; Zhang, Dawei; Minhas, Badar; Qian, Hongchang; Terryn, Herman A.; Mol, Johannes M.C.

DOI
10.1016/j.jmst.2019.12.008

Publication date
2021

Document Version
Final published version

Published in
Journal of Materials Science and Technology

Journal of Materials Science & Technology 64 (2021) 57–65

Contents lists available at ScienceDirect

Journal of Materials Science & Technology

journal homepage: www.jmst.org

Research article

Long-term deterioration of lubricant-infused nanoporous anodic aluminium oxide surface immersed in NaCl solution

Dequan Wu [a], Lingwei Ma [a], Bei Liu [a], Dawei Zhang [a,*], Badar Minhas [a], Hongchang Qian [a], Herman A. Terryn [b,c], Johannes M.C. Mol [c]

[a] Beijing Advanced Innovation Centre for Materials Genome Engineering, Institute for Advanced Materials and Technology, University of Science and Technology Beijing, Beijing 100083, China
[b] Department of Materials and Chemistry, Research Group Electrochemical and Surface Engineering, Vrije Universiteit Brussel, Brussels, Belgium
[c] Department of Materials Science and Engineering, Delft University of Technology, Delft, the Netherlands

ARTICLE INFO

Article history:
Received 28 October 2019
Received in revised form
30 November 2019
Accepted 3 December 2019
Available online 8 January 2020

Keywords:
Lubricant-infused surface
Anodic aluminium oxide
Deterioration
EIS

ABSTRACT

This study investigated the deterioration of a lubricant-infused anodic aluminium oxide surface in a 1 M NaCl solution for ~200 days. Direct observation by cryo-SEM and quantitative analyses by UV spectroscopy and EIS revealed that the long-term deterioration of the lubricant-infused surface was divided into two stages: the surface-adhered lubricant layer gradually dissolved at a constant rate until the substrate was exposed; afterwards the lubricant infused in the nanochannels began to diffuse and was depleted after ~200 days. The EIS results also revealed that the defects reduced the corrosion resistance of the lubricant-infused surface considerably.

1. Introduction

Creating durable surfaces for aluminium and its alloys that withstand corrosion in underwater environments is of great importance for marine and energy-related applications [1–3]. Surface anodization has been widely used to improve the corrosion resistance of aluminium by forming protective anodic aluminium oxides (AAO) consisting of a thin and compact barrier layer and a thick porous layer [4,5]. However, the high-aspect-ratio nanochannels of the porous layer is prone to absorb and retain corrosive media [6]. To solve this problem, various materials have been used to seal the pores including chromates, nickel salts, organic acids and sol-gels [7,8]. Lubricants such as high-viscosity oils or greases have also been used as sealing materials to improve surface lubricity under tribological environment [9,10]. Nevertheless, the effect of lubricant-sealing on the corrosion resistance is rarely reported.

Inspired by Nepenthes pitcher plants, a new type of surface called the lubricant-infused surface (LIS) or slippery liquid-infused porous surface (SLIPS) has been invented by infusing lubricant with low surface energy into porous micro/nanostructures [11,12]. The capillary force of the rough nanostructure locks the lubricant in the porous substrate, forming a continuous and smooth lubricant surface [13,14]. The low surface energy of the liquid lubricant enables the surface a slippery feature useful for the reduction of water condensation, microbial fouling and ice nucleation [15,16]. Additionally, the seamless feature of the hydrophobic lubricant layer may also protect the substrate from being attacked by external corrosive media, making LIS/SLIPS an emerging surface technology for wide potential applications in corrosive underwater conditions [17–20]. Generally, the criteria of designing a LIS are extremely rigorous: i) the lubricant must fully wet the micro-/nanoporous surface of the LIS substrate; ii) the lubricant is immiscible with the fluids it contacts; and iii) the contacting fluids cannot penetrate into the LIS substrate [21–23].

Recent studies have shown an increasing interest in developing LIS/SLIPS on various metal substrates such as aluminium, magnesium, zinc and steels for enhanced corrosion protection [24–28]. For example, Wang et al. have developed a LIS by infusing perfluoropolyether (PFPE) lubricant into a superhydrophobic hydrothermally-treated zinc surface [17]. After 10 days of immersion in the NaCl solution, the LIS exhibited a more stable barrier property than the superhydrophobic surface in which the protective air layer could be rapidly replaced by the aqueous solution. More recently, LIS was prepared by infusing PFPE into the layer-double hydroxide (LDH) film grown on the plasma electrolytic oxidised AZ91D magnesium alloy. From polarisation tests, the cor-

* Corresponding author.
E-mail address: dzhang@ustb.edu.cn (D. Zhang).

https://doi.org/10.1016/j.jmst.2019.12.008
1005-0302/

rosion rate of the LIS-protected AZ91D was five orders of magnitude lower than the bare metal, and two orders of magnitude lower than the metal protected by a similarly prepared superhydrophobic surface [27].

At present most studies in this field focus on the fabrication of the LIS/SLIPS with delicate microstructures or superior functional performances, whereas the long-term stability and degradation of the LIS/SLIPS in the proposed service environment has rarely been studied. For example, the LISs prepared for corrosion protection [29,30] or anti-fouling applications [23,31] have been studied only for a short period of time ranging from several days to weeks. However, because of the high mobility of the liquid lubricant, the stability of LIS/SLIPS as a protective or functional surface during long-term environmental exposure is questionable [32–34]. Partial dissolution, which is a commonly observed phenomenon between organic and aqueous liquids, may result in a slow lubricant loss during long-term immersion [35,36] For example, typical lubricants such as Krytox for LIS preparation were measured with a solubility ranging from several nanograms to milligrams per litre in water [37–39]. Weak fluctuation and anisotropic pressure of the immersing solution may further promote the diffusion of the liquid lubricant even in static underwater conditions [40]. In addition, some silicone-based and Krytox-based lubricants, which have high water immiscibility and are widely used in LIS development, have been also found to cloak the deposited water and be removed as water slides off from the surface [41–43]. More importantly, quantitative and in situ analytical techniques by which the extent of LIS/SLIPS deterioration can be monitored under immersed conditions have seldomly been reported. Due to the liquid nature of the infused lubricant, it is also difficult to directly observe the loss of lubricant from the porous substrate [46]. Although several studies have shown that the surface hydrophobicity would deteriorate due to the depletion of the infused lubricant [44], it has been difficult to identify the quantity of the lost lubricant and the transition point from water sliding to water pinning on the surface [41].

We have recently reported the development of LIS by infusing mineral oil lubricant into the high-aspect-ratio nanochannels of AAO surface via a vacuum impregnation method [45]. The work highlighted the importance of rational design in the LIS preparation and the vacuum impregnation method which was proved to be more efficient in filling deep pores than simple immersion. The obtained surface demonstrated self-healing effects against mechanical damages (e.g. wearing and cracking) and an improved corrosion resistance over a relatively short exposure (85 days) under aqueous immersion.

In the present study, we aimed to understand the degradation mechanism of this type of LIS under long-term immersion in 1 M NaCl solution for over 200 days by carrying out a combination of microscopic, spectroscopic and electrochemical analyses. During the immersion, the change in the surface hydrophobicity of the LIS was evaluated by water contact angle measurements. The lubricant loss of the LIS was tracked by direct observation using cryogenic scanning electron microscopy (cryo-SEM) and confirmed by ultraviolet (UV) spectroscopy. Electrochemical impedance spectroscopy (EIS) was employed as an in situ measurement technique to correlate the loss of lubricant with the degradation of the protective properties.

2. Experimental

2.1. Materials

Rolled aluminium foils with a purity of 99.999 wt.% were purchased from the Beijing Institute of Nonferrous Metals (China). A mineral oil lubricant (Shell Advanced AX5, Shell) was purchased from Shell Global. Deionised water was used in all the experiments. Other chemical reagents employed in this work were purchased from Sinopharm and were of analytical grade.

2.2. LIS preparation

AAO was fabricated by a two-step anodising method. The first anodisation step was performed in 0.3 M phosphoric acid at 195 V via a DC source (N8741, Keysight, Ameirca) using an electropolished aluminium foil as the anode and a degreased aluminium foil as the cathode. After 60 min, the first anodic film was immersed in a mixture solution (6 wt.% phosphoric acid, 1.8 wt.% chromic acid, and deionised water) at 60 °C for 30 min. Then, the second anodisation step was performed under the same conditions for 2 h. The obtained AAO has a pore diameter of ~200 nm and a pore depth of ~50 μm as observed by SEM.

The LIS was fabricated by infusing the lubricant into the AAO nanochannel structure through a vacuum impregnation method, as described in our previous study [45]. The fabrication process can be described briefly as follows. The AAO specimens were placed in a vacuum chamber (~3 Pa) for 5 h to completely remove the air in the container and nanochannels. Subsequently, oil was injected into the container, and the oil covered the AAO specimen. After soaking in vacuum condition for 1 h, the lubricant infused into the nanochannels without the resistance of compressed air trapped in pores. When the vacuum chamber was refilled with air, the atmospheric pressure further pushed the lubricant to deeply infuse into the nanochannels.

2.3. Cryo-SEM

Cryo-SEM was carried out using a microscope (FEI Helios NanoLab G3 UC) to observe the solid–liquid interface of the LIS directly. First, the specimen was fixed to a copper holder using conductive glue and mounted on a cryo-cell holder. Then, the cryo-cell holder was plunged into liquid nitrogen for ~10 s to freeze the infused oil. The specimen was bent reciprocally by tweezers to break the specimen and expose a fresh cross section. The cryo-cell holder was then transferred into the specimen chamber, which was pre-frozen to −140 °C. Before the observation, the specimen should be sublimated at −90 °C for 25 min to remove the ice crystals formed during liquid nitrogen submersion. After this, the cryo-SEM observation chamber was maintained at a pressure of $\sim 1.02 \times 10^{-4}$ Pa and a temperature of −140 °C. Then, the specimen was sprayed with gold at a current strength of 10 mA for 60 s. The LIS was milled by a focused ion beam (FIB) at a beam energy of 30 keV and a current strength of 2.5 nA with a dwell time of 100 ns per pixel. Next, the specimen was sprayed with gold again. SEM images were obtained by using backscattered electrons (2 keV and 60 pA).

2.4. Surface wettability

The sessile water contact angle (WCA) and sliding angle (SA) were measured using a contact angle meter (OCA20, Dataphysics) to evaluate the surface wettability of the specimens. The specimens (~1 cm in diameter), which were immersed in the 1 M NaCl solution, were retrieved and air dried for 30 min. The sessile WCA was measured by placing a deionised water droplet (~5 μL) on the specimen surface. The SA was recorded by tilting the surface slowly until a 10 μL water droplet could slide off. The results were obtained by averaging five measurements on different areas of the specimens.

2.5. Electrochemical tests

EIS measurements were performed using a potentiostat/galvanostat (PARSTAT 2273, Princeton Applied Research)

as an in situ method to track the lubricant loss under immersion in the 1 M NaCl solution at 25 °C. The LIS specimen (~1 cm in diameter) was the working electrode. The reference and counter electrodes were a saturated calomel electrode and Pt foil, respectively. The impedance spectra were measured in the range of 10^{-2}–10^{5} Hz with an amplitude of 20 mV. To simulate the inner structure of the LIS, data fitting was carried out using ZSimpWin software. All the tests were performed at least twice to verify reproducibility.

2.6. UV spectroscopy

UV spectroscopy was carried out using a spectrophotometer (U3900H, Hitachi) to measure the quantity of oil remaining in the LIS specimens. Dichloromethane was used as an extraction solvent to dissolve the lubricant in the LIS and as a reference blank solution to measure absorbance. The specimens immersed in the NaCl solution for different times were retrieved and then submerged in 5 mL dichloromethane under ultrasonication for lubricant extraction. The extraction solution was then injected into a quartz dish and scanned under the spectrophotometer. To obtain the relationship between the oil concentration and peak intensity, a series of standard oil solutions (lubricant concentration: 0, 0.4, 0.8, 1.2, 1.6, 2, 2.4, 2.8, 3.2, 3.6, 4 mg/mL) were prepared and tested.

3. Results and discussion

3.1. Cryo-SEM morphology

To study the deterioration of the LIS, cryo-SEM was employed for directly observing the top view and cross section of the LIS during the long-term immersion. Cryo-SEM allows to image the liquid lubricant in its frozen condition, which cannot be realized by conventional SEM or optical microscopy. As shown in Fig. 1(a1) and (a2), the as-prepared LIS specimen consisted of the AAO substrate covered by a continuous and smooth lubricant layer with a thickness of ~7 μm. After immersion in the NaCl solution for 20 days (Fig. 1(b1) and (b2)), the lubricant layer decreased slightly in thickness and remained largely continuous, although less lubricant coverage was observed in local spots. After 60 days, the nanoporous surface was exposed and some pores became visible in the top view of the surface (Fig. 1(c1)), suggesting that the surface lubricant layer was completely lost. However, the cross-sectional view (Fig. 1(c2)) indicated that the nanochannels were still almost fully filled with the lubricant at this stage.

After 90 days of immersion, all pores on the AAO surface were exposed (Fig. 2(a1)) and the cross section showed that a few microns of the infused lubricant were released from the nanochannels (Fig. 2(a2)). After 150 days of immersion, a rough porous AAO surface was observed (Fig. 2(b1)) and the cross section (Fig. 2(b2)) showed that the lubricant had been released from pores with depths of 20–30 μm. The lubricant in the upper portion (Fig. 2(b3)) of the LIS was largely depleted, whereas the nanochannel in the bottom portion (Fig. 2(b4)) was still filled with the lubricant. After 210 days, the lubricant had further depleted from the nanochannels, many of which became completely empty (Fig. 2(c)).

3.2. Surface wettability

The WCA reflects the surface wettability, which is determined by the chemical composition and roughness of the underlying substrate [46]. As shown in Fig. 3(a), when a smooth lubricant layer fully covered the AAO surface, the WCA on the initial LIS was ~99.5°. When the surface-adhered lubricant was completely wiped off, the water droplet contacted with a composite surface consisting of the exposed aluminium oxide surface and the lubricant filled in the AAO nanochannels. The corresponding WCA decreased to ~76°. When the lubricant was partially removed from the nanochannels, the water droplet was essentially in contact with the porous surface of AAO, which consisted of aluminium oxide and the air trapped inside the nanochannels. The WCA in this case was ~68°. Therefore, the deterioration of the surface conditions of the LIS can be indirectly estimated up to a certain stage by the variation of the WCA. Fig. 3(b) shows the WCA of the LIS after immersion in the 1 M NaCl solution for different times. After 1 day of immersion, the WCA decreased from ~99° to 87°, which might be attributed to the residual moisture on the lubricant surface after immersion. The WCA continued to decrease slightly in the following 60 days. From the 60th day to the 90th day of immersion, the WCA decreased remarkably from 78° to 69°, which was attributed to the exposure of the AAO porous substrate. It is noteworthy that the two divided colours in Fig. 3(c) indicated that the transition from the dissolution of surface-adhered lubricant layer to the exposure of AAO substrate took place somewhere between the 60th day and 90th day in the immersion. The WCA almost levelled off at 65° after 120 days. The further release of the lubricant stored in the interior nanochannels could not be detected by the WCA because the WCA reflects only the surface wettability. As shown in Fig. 3(c), the SA of the LIS increased from ~10° to ~85° during the initial 60 days of immersion. On the 90th day, the water droplets were found to be pinned on the LIS, even when the LIS was tilted by 90°. The transition from droplet sliding to droplet pinning indicated the exhaustion of the top lubricant layer and the exposure of the porous AAO substrate. Based on the combination of the WCA measurement and the direct observation by cryo-SEM, the LIS deterioration process can be divided into two stages, i.e. the dissolution of the surface-adhered lubricant layer, and the leaching of the lubricant infused in the nanochannels during the subsequent immersion.

3.3. Lubricant loss determined by UV spectroscopy

UV spectroscopy was used to provide a more accurate quantification of the lubricant loss during the long-term immersion. Because the UV absorption is directly proportional to the solution concentration according to the Beer–Lambert law [47], a quantitative relationship can be established between the UV absorbance and lubricant concentration to quantify the lubricant in pores. Fig. 4(a) shows the normalised UV spectra of the LIS with different concentrations of the lubricant extracted from the AAO pores in dichloromethane. The typical absorption wavelengths of the lubricant were in the range of 220−400 nm, and the characteristic peak was chosen to be 282 nm. The linear correlation between the absorbance and lubricant concentration is shown in Fig. 4(b). Fig. 4(c) shows the variation in the UV spectra of the lubricant extracted from the LIS after different immersion times. Based on these spectra, the amount of lubricant remaining in the LIS nanopores was estimated. The quantity of the lubricant was found to decrease at a constant rate in the first 60 days of immersion (Fig. 4(d)). Associated with the variation of the surface wettability (Fig. 3), the mass loss during this period could be attributed to the dissolution of the surface-adhered lubricant layer. After 60 days, the rate of mass loss of the lubricant in the LIS specimen slowed down. From 180–210 days, only ~2.7 mg of lubricant residue was left in the nanochannels.

3.4. EIS measurements

EIS has been frequently used to detect information pertaining to the surface/interface of bare and coated metals [48]. In this study, EIS was used to understand the deterioration process of the LIS during long-term immersion. Unlike UV spectroscopy, which reflects the lubricant loss in the entire specimen, EIS can detect the dete-

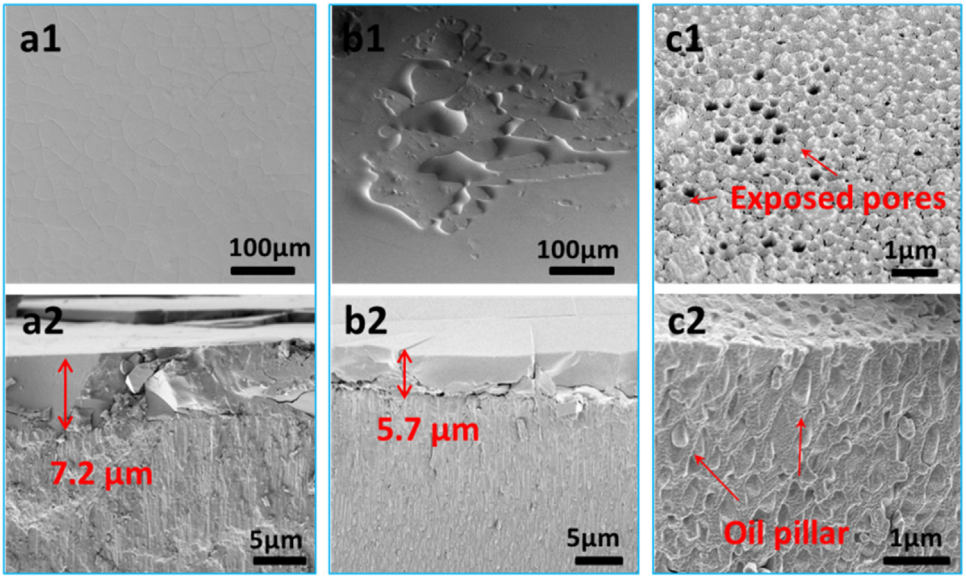

Fig. 1. Cryo-SEM images showing (1) top view and (2) cross section of LIS during immersion in 1 M NaCl solution for (a) 0, (b) 20, and (c) 60 days.

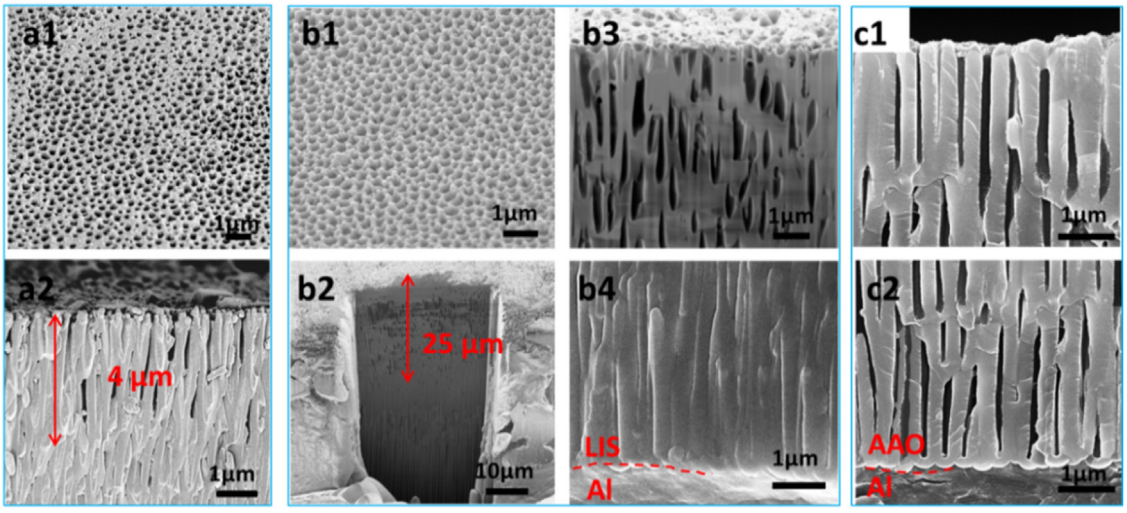

Fig. 2. Cryo-SEM image of LIS during immersion in 1 M NaCl solution for 90 (a), 150 (b) and 210 (c) days. (a1) Top view, (a2) upper cross section. (b1) Top view, (b2) entire cross section, (b3) upper cross section, and (b4) bottom cross section. (c1) Upper cross section, (c2) bottom cross section.

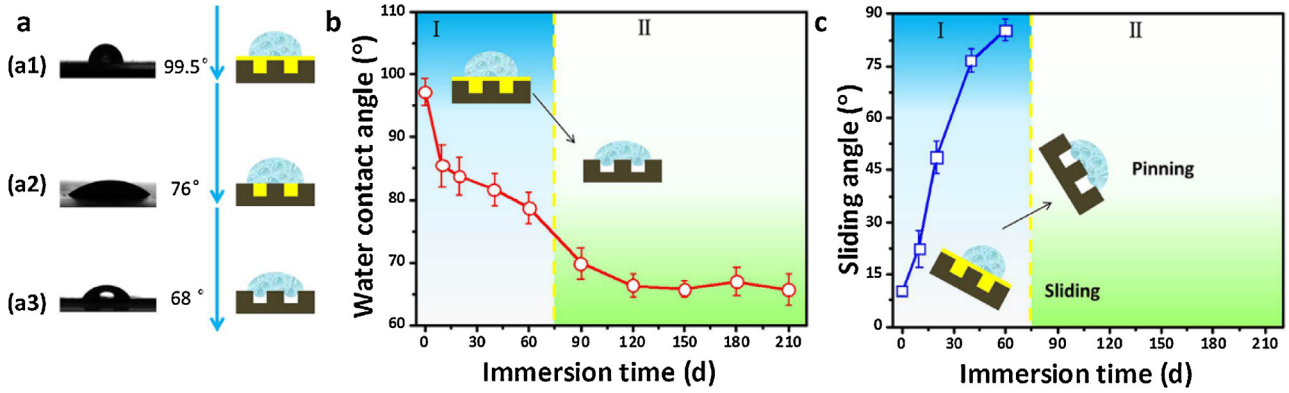

Fig. 3. (a) WCA on surface covered by oil layer (a1), solid and oil composite surface (a2), and solid and air composite surface (a3). WCA (b) and SA (c) of LIS during different deterioration stages.

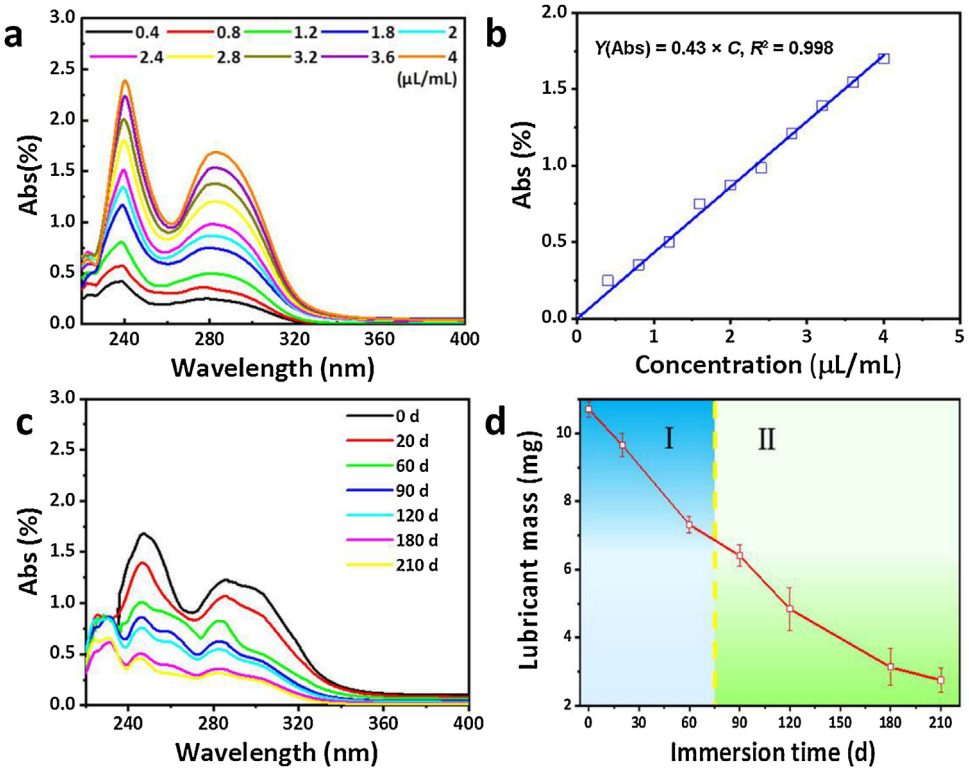

Fig. 4. Change in lubricant mass of LIS during long-term immersion. (a) UV absorption spectra of standard lubricant solutions with different lubricant concentrations (0.4, 0.8, 1.2, 1.6, 2.0, 2.4, 2.8, 3.2, 3.6, and 4.0 μL/mL) in dichloromethane, (b) linear correlation between UV absorption intensity and lubricant concentration, (c) UV absorption spectra of extracted lubricant in dichloromethane, (d) change in lubricant mass in LIS during deterioration process.

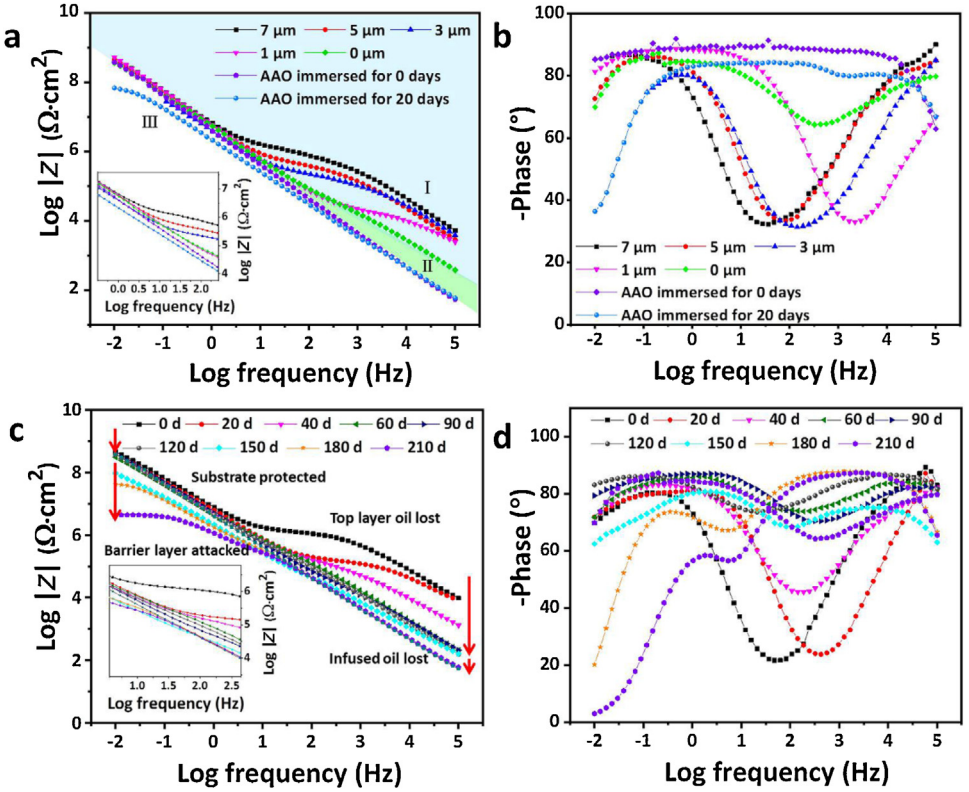

Fig. 5. (a) Impedance modulus plots and (b) phase angle plots for LIS with controlled top layer lubricant thicknesses (0, 1, 3, 5 and 7 μm), bare AAO immersed in 1 M NaCl solution for 0 day (the NaCl solution was just infused into the nanochannel), and bare AAO immersed in 1 M NaCl solution for 20 days. (c) Impedance modulus plots and (d) phase angle plots of LIS during immersion in 1 M NaCl solution for up to 210 days.

rioration of the protective property of the LIS even in a very small area. To more clearly identify the deterioration stages, EIS was first carried out on the LIS with excess surface lubricant of different thicknesses (0–7 μm) to simulate the gradual loss of surface lubricant. Additionally, the immersion solution (1 M NaCl solution) was infused into the nanochannels of bare AAO to simulate the situation in which the impregnated lubricant had completely diffused out of the nanochannels, and the bare AAO was immersed in the 1 M NaCl solution for 20 days to simulate the situation in which the barrier layer was attacked. The EIS results for these standard specimens are shown in Fig. 5(a) and (b). According to previous studies on sealed AAO such as those by chromates or hydrothermal treatment, the low-frequency range of the impedance spectra mainly reflected the inner barrier layer of AAO, whereas the high-frequency range corresponded to the outer porous layer [49,50]. In Fig. 5(a), the impedance moduli value in the high-frequency region declined as the thickness of the surface oil layer decreased [51]. In Fig. 5(b), the phase angle plots of the LIS show two time constants: the crest in the high frequencies refers to the lubricant layer, and the crest in the low frequencies refers to the barrier layer [52]. When the pores were infused with the NaCl solution, the impedance modulus plot (Fig. 5(a)) became a straight line and only one time constant could be observed over the entire measured frequencies [53,54]. After AAO was immersed in the 1 M NaCl solution for 20 days, the modulus value in the low frequencies decreased remarkably, indicating corrosion of the barrier layer [55]. Based on the EIS results, the deterioration of the protective property of the LIS could be divided into three stages: (I) the dissolution of the surface-adhered lubricant until the substrate was exposed, (II) the diffusion of the infused lubricant from the AAO nanochannels until the barrier layer was exposed, and (III) the corrosion attack of the barrier layer.

Fig. 5(c) and (d) show the EIS results for the LIS prepared in this study over 200 days of immersion in the 1 M NaCl solution. In the first 60 days, the impedance moduli in the high-frequency region (Fig. 5(c)) declined clearly, which was attributed to the dissolution of the top layer lubricant covering the LIS [52]. This result agreed well with the cryo-SEM observation in Fig. 1. From 90–210 days, the impedance moduli in the high-frequency region (Fig. 5(c)) declined gradually, which was attributed to the continuous loss of the lubricant from the pores. The corresponding phase angle plots in Fig. 5(d) show that the crest in the high frequencies flattened as a function of immersion time, which also indicated the loss of the lubricant layer. However, the impedance moduli in the high-frequency region did not disappear completely. The existing time constants in the high-frequency region (Fig. 5(d)) indicated that some lubricant still remained in the nanochannels. These results agreed with those obtained by UV spectroscopy. As shown in Fig. 5(c), the impedance modulus plots in the low-frequency region overlapped with the $|Z|_{0.01\mathrm{Hz}}$ values remained almost unchanged and the phase angle in the low-frequency region remained at a high value of around ~80° during the entire duration of 120 days, indicating that the barrier layer was well protected by the infused lubricant in the initial time. After 150 days, a major decrease was observed in the $|Z|_{0.01\mathrm{Hz}}$ value and the phase angle in the low-frequency region decreased to ~50°, suggesting that the barrier layer of the AAO film was attacked [55].

Noticeably, the fact that $|Z|_{0.01\ \mathrm{Hz}}$ values began to decrease after 150 days of immersion did not agree with the observations from cryo-SEM or UV spectroscopy, which indicated that the nanochannels became empty after 210 days of immersion, before which the barrier layer of AAO might have been protected by the lubricant left in the nanochannels. We postulated that this discrepancy was caused by the defects in the AAO surface [55]. During fabrication or storage, the formation of pore defects or cracks in the AAO nanopore array is inevitable. The surface may also have cracks from which the lubricant could more rapidly leach out [5]. By using cryo-SEM, we found that in the initial stage of immersion (Fig. 6(a) and (b)), the nanochannels of AAO and the defects could all be filled by the liquid lubricant, making it difficult to differentiate them by EIS. In the later stage of immersion period, as the top lubricant layer disappeared, the oil could deplete from the cracks more rapidly because the size of the cracks was considerably larger than that of the nanochannels (Fig. 6(c) and (d)), making the damaged aluminium substrate expose to the NaCl solution finally.

To confirm that the decreased corrosion resistance after 150 days of immersion was indeed the result of the surface defects, additional EIS tests were performed on LIS specimens that were artificially cracked by bending them around a cylinder with a diameter of 5 mm. To simulate the different stages of the deterioration, the depletion of the lubricant from the cracked LIS was accelerated by placing it under flowing water for 10 min or by carrying out ultrasonication for 10 min. For comparison, we also infused the 1 M NaCl solution into a cracked empty AAO surface (without employing surface protection or impregnating the surface with a lubricant). As shown in Fig. 7(a), the cracked LIS exhibited clear impedance moduli in the high-frequency region, which indicates the coverage of the surface by the lubricant layer. After the specimen was washed or ultrasonically treated, the lubricant stored in the cracks released quickly and the partial lubricant locked in the nanochannels still remained, which resulted in the diminishing of the impedance moduli. When the lubricant was lost completely and replaced by the NaCl solution (as shown in the plot labelled as 'AAO-solution infusion' in Fig. 7), the high-frequency region of the Impedance modulus plot almost became a straight line. In the low-frequency region, the Impedance modulus plot of the cracked LIS overlapped with that of the LIS because the cracks were covered by the lubricant flowing into them [4◦]. After the cracked LIS was washed or ultrasonically treated, the cracks or damaged barrier layer were exposed to the solution, leading to a major decrease in the $|Z|_{0.01\mathrm{Hz}}$ value compared to the corresponding value for the undamaged AAO. These results showed that the existence of cracks could be detected by EIS even when the LIS had not completely deteriorated.

Cryo-SEM, UV spectroscopy, and EIS have different advantages/limitations in the study of LIS deterioration. The cryo-SEM method can provide surface and cross-sectional inspection of the lubricant infused in small area (even in individual nanochannels), but the detection of defects hidden in the nanopore array is not easy. UV spectroscopy measures the amount of lubricant in the entire film including the surface adhered lubricant layer and the amount of lubricant trapped in the nanochannels or cracks. In contrast, EIS can detect small defects in the LIS owing to the low-frequency impedance, which is often used to reflect the onset of corrosion and the deterioration of the protective property of the LIS.

EIS can also be used to quantitatively assess the degradation of the LIS by fitting the EIS results in the form of equivalent circuits, as shown in Fig. 8. Because of the presence of inhomogeneity in the barrier and porous layers, their capacitive behaviours were better simulated by constant phase elements (Q) than by simple capacitances (C). The relationship between Q and C is described in Eq. 1 [56,57],

$$C = Q^{1/n} R^{(1-n)/n} \tag{1}$$

where values of n are a dispersion index describing the non-ideal behaviour of capacitance ($n = 1$, Q refers to a real homogeneous capacitance; $n = 0$, Q refers to a resistance) [53].

It is well known that an anodic oxide film consists of a thin inner barrier layer and a thick outer porous layer. The porous layer is composed of pores and walls in the shape of hexagonal cells. Therefore, the oxide film can be modelled by the equivalent circuit shown in Fig. 8(a). This circuit has been previously used for AAO with sealed pores obtained by hydrothermal treatment or chemical deposition [58–60]. In this circuit, R_s is the solution resistance. R_w and Q_w are

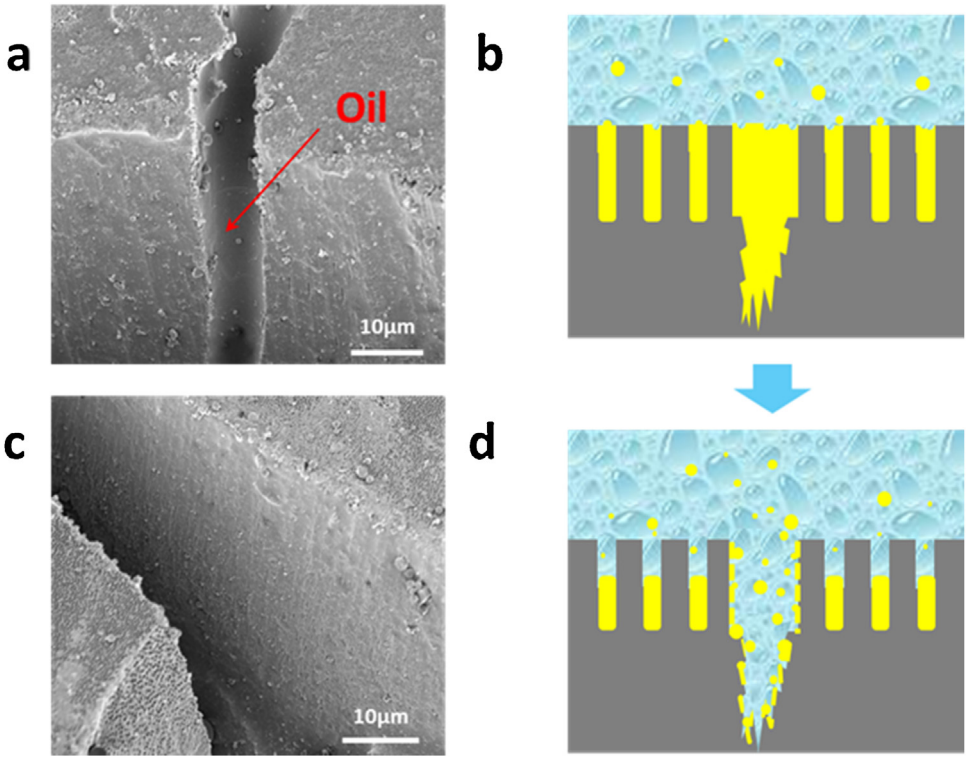

Fig. 6. Deterioration process of cracked LIS. (a, b) Cracks and nanochannels in LIS still filled with lubricant after immersion in 1 M NaCl solution for 60 days. (c, d) lubricant dissolved from nanochannels partially but from cracks predominantly after immersion in NaCl solution for 150 days.

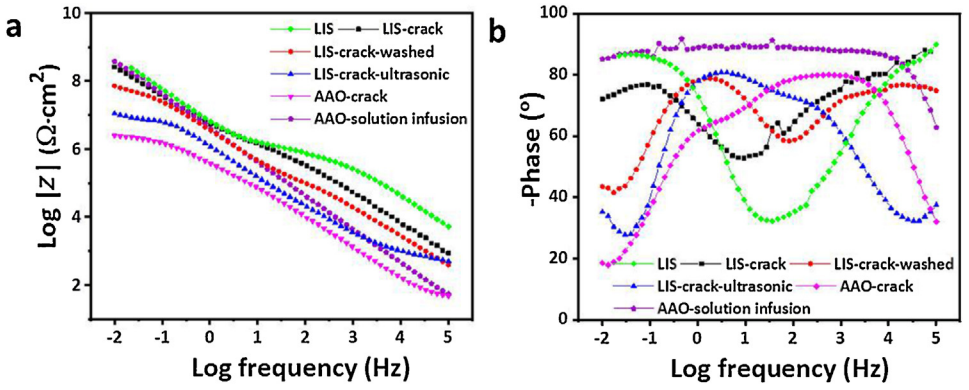

Fig. 7. (a) Impedance modulus plots and (b) phase angle plots of standard specimens (intact and cracked) to simulate deterioration process of defective LIS.

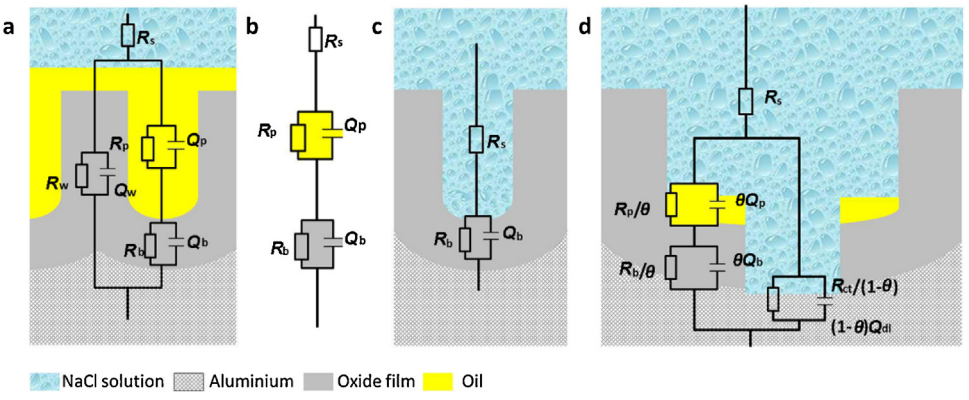

Fig. 8. Equivalent circuits for modelling impedance behaviour of LIS in different deterioration stages. (a) Nanochannels infused with lubricant, (b) simplified circuit of (a), (c) nanochannels fully penetrated by NaCl solution, and (d) attack occurring on barrier layer.

Table 1
Electrochemical parameters fitted from EIS results of LIS immersed in 1 M NaCl solution from 0 to 120 days.

Time (d)	Q_p ($\times10^{-10}$ S s^n cm^{-2})	n	C_p ($\times10^{-10}$ S s^n cm^{-2})	R_p ($\times10^3$ Ω cm^2)	Q_b ($\times10^{-10}$ S s^n cm^{-2})	n	C_b ($\times10^{-10}$ S s^n cm^{-2})	R_b ($\times10^9$ Ω cm^2)	χ^2
0	7.38	0.89	3.08	1175	242	0.90	377	2.24	4.5×10^{-3}
20	17.7	0.98	15.3	474.3	308	0.84	675	1.99	2.1×10^{-3}
40	139	0.82	34.7	128.6	369	0.92	549	2.63	6.2×10^{-4}
60	904	0.89	431	27.47	409	0.95	503	1.26	3.3×10^{-4}
90	752	0.98	658	18.7	443	0.92	659	2.16	3.2×10^{-3}
120	2674	0.95	2018	17.9	447	0.94	610	2.91	7.8×10^{-3}

Table 2
Electrochemical parameters fitted from EIS results of LIS immersed in 1 M NaCl solution from 150 to 210 days.

Time (d)	θQ_p ($\times10^{-10}$ S s^n cm^{-2})	n	θC_p ($\times10^{-10}$ S s^n cm^{-2})	R_p/θ ($\times10^3$ Ω cm^2)	θQ_b ($\times10^{-10}$ S s^n cm^{-2})	n	θC_b ($\times10^{-10}$ S s^n cm^{-2})	R_b/θ($\times10^9$ Ω cm^2)
150	2566	0.80	778	33.0	685	0.95	814	0.39
80	18410	0.67	4640	33.1	738	0.87	1297	0.59
210	12460	0.85	6187	15.2	1650	0.64	14251	0.28
(1-θ)Q_{dl}($\times10^{-10}$ S s^n cm^{-2})	n	(1-θ)C_d ($_l\times10^{-6}$ S s^n cm^{-2})	$R_{ct}/(1-\theta)$ ($\times10^6$ Ω cm^2)	χ^2				
284	0.72	126	6110	2.2×10^{-4}				
404	0.97	5.02	288	4.3×10^{-4}				
416	0.97	4.55	4.55	3.1×10^{-4}				

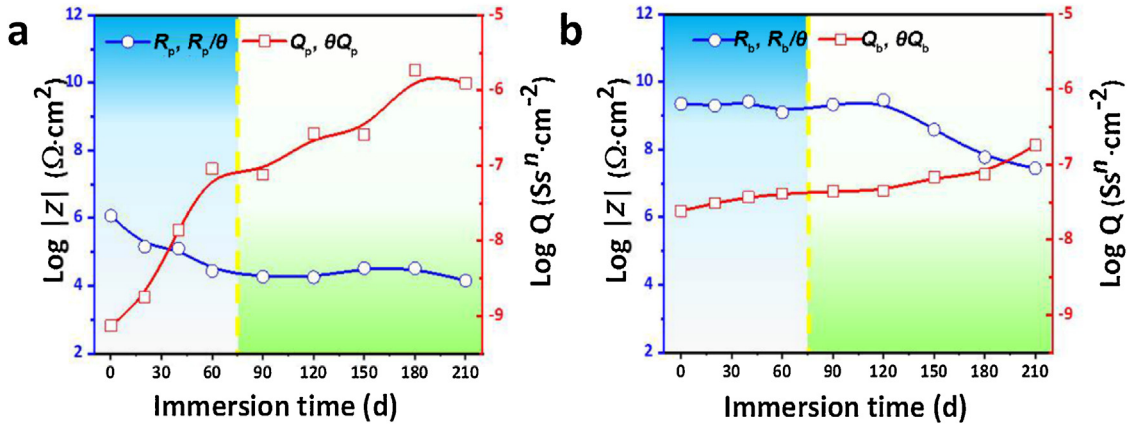

Fig. 9. Fitting results of parameters (R (or θR) and C (or θC)) of (a) lubricant in porous layer and (b) barrier layer during immersion in 1 M NaCl solution for 210 days.

the resistance and capacitance of the hexagonal pore walls, respectively. R_b and Q_b are the resistance and capacitance of the barrier layer, respectively. R_p and Q_p are the resistance and capacitance of the lubricant in the porous layer, respectively. R_w and Q_w are usually omitted because R_w is very high and Q_w is low for the AAO pore walls [61,62]. Therefore, the equivalent circuit can be simplified as illustrated in Fig. 8(b). For a completely deteriorated LIS, the lubricant in the nanochannel was entirely replaced by the NaCl solution. The porous layer could not be detected by the EIS because of the high conductivity of the NaCl solution inside the nanochannels. Therefore, the equivalent circuit element that referred to the porous layer was ignored [58], as shown in Fig. 8(c). Pitting corrosion or cracks could occur on the barrier layer at the bottom of the nanochannels. Such surface inhomogeneities could be modelled by introducing a parameter θ to represent the fraction of the surface covered by the intact barrier layer and a parameter (1-θ) to represent the fraction of the defective or corroded surface [54,55] (Fig. 8(d)). In this case, the double-layer capacitance Q_{dl} and charge transfer resistance R_{ct} should be taken into account for the active corrosion on the damaged barrier layer. When $\theta = 1$, the barrier layers are not damaged. The aluminium surface is entirely covered by the anodic film, so R_{ct} and Q_{dl} do not exist. When θ is close to 0, the porous and barrier layers are completely removed and the equivalent circuits represent the exposure of the aluminium substrate.

Tables 1 and 2 summarized the electrochemical parameters for the LIS by fitting the EIS results using the equivalent circuits in Fig. 8(b) and (d), respectively. The small value of χ^2 indicated that the EIS results were well fitted. The values of n varied from ~0.7 to ~1. Fig. 9(a) and (b) illustrated the fitting parameters from the EIS results as a function of time. In Fig. 9(a), the capacitance of the lubricant (C_p or θC_p) increased and the resistance (R_p or θR_p) decreased at a relatively constant rate during the initial 60 days of immersion; this corresponded to the continuous deterioration of the surface lubricant layer. These results agreed well with the cryo-SEM and UV spectroscopy results. After 60 days, the change in the capacitance and resistance of the lubricant slowed down. For the inner barrier layer structure (Fig. 9(b)), the capacitance (C_b) and resistance (R_b) remained almost unchanged until 120 days of immersion, indicating that the barrier layer was well protected.

After 120 days, the resistance (R_b or θR_b) decreased and the capacitance (C_b or θC_b) increased clearly, which indicated that the barrier layer was progressively attacked.

4. Conclusion

In this study, the deterioration process of a typical LIS, prepared by infusing the nanopores of AAO with mineral oil, was investigated under long-term immersion in 1 M NaCl solution for over 200 days, using a combined microscopic, spectroscopic and electrochemical approach involving surface wettability analysis, cryo-SEM observations, UV spectroscopy measurements, and EIS measurements. The loss of the lubricant from the surface and nanochannels was quantitatively studied. The results showed that the deterioration of the LIS could be divided into the following stages: in the first stage, the smooth surface lubricant layer gradually dissolved at a relatively constant rate until the porous AAO substrate got exposed. In the second stage, the diminishing of the impedance moduli in the high-frequency region of the EIS results indicated the continuously dissolution of lubricant infused in the nanochannels. The decrease in the $|Z|_{0.01\ Hz}$ in this stage implied that defects such as cracks on the LIS, which were initially masked in the electrochemical response by sufficient lubricant filling of the defect areas, were exposed and penetrated by the NaCl solution. Consequently, the barrier layer under the defects was preferentially attacked much earlier than the complete depletion of the lubricant from the nanochannels (~210 days). The results from this study provided comprehensive insights of how a typical LIS could deteriorate under long-term immersion. A root-cause analysis was conducted to highlight the significant impact of AAO defects on the corrosion resistance of the LIS. These understandings would be highly useful in light of the growing interest in LIS and particularly their applications for underwater corrosion protection.

Acknowledgements

This work was supported by the National Key Research and Development Program of China (No. 2016YFE0203600), the National Natural Science Foundation of China (No. 51771029), the Beijing Nova Program (Z171100001117076) and the 111 Project (B17003).

References

[1] L.Y. Cui, H.P. Liu, W.L. Zhang, Z.Z. Han, M.X. Deng, R.C. Zeng, S.Q. Li, Z.L. Wang, J. Mater. Sci. Technol. 33 (2017) 1263–1271.
[2] L. Guo, W. u, Y.F. Zhou, F. Zhang, R.C. Zeng, J.M. Zeng, J. Mater. Sci. Technol. 34 (2018) 1455–1466.
[3] Y. Huang, L. Deng, P. Ju, L. Huang, H. Qian, D. Zhang, X. Li, H.A. Terryn, J.M.C. Mol, ACS Appl. Mater. Interface 10 (2018) 23369–23379.
[4] C.S. Chi, J.H. Lee, I. Kim, H.J. Oh, J. Mater. Sci. Technol. 31 (2015) 751–758.
[5] J. Lee, S. Shin, Y. Jiang, C. Jeong, H.A. Stone, C. Choi,Adv. Funct. Mater. 27 (2017), 16066040.
[6] J. Lee, U. Jung, W. Kim, W. Chung, Appl. Surf. Sci. 283 (2013) 941–946.
[7] J. Lee, D. Kim, C. Choi, W. Chung, Nano Energy 31 (2017) 504–513.
[8] T.P. Hoar, G.C. Wood, Electrochim. Acta 7 (1962) 333–353.
[9] H. Wang, H. Yi, H. Wang, Appl. Surf. Sci. 252 (2005) 1662–1667.
[10] W. Zhang, D. Zhang, Y. Le, L. Li, B. Ou, Appl. Surf. Sci. 255 (2008) 2671–2674.
[11] T.S. Wong, S.H. Kang, S.K. Tang, E.J. Smythe, B.D. Hatton, A. Grinthal, J. Aizenberg, Nature 477 (2011) 443.
[12] M. Nosonovsky, Nature 477 (2011) 412–413.
[13] C. Zhang, B. Zhang, H. Ma, Z. Li, X. Xiao, Y. Zhang, X. Cui, C. Yu, M. Cao, L. Jiang, ACS Nano 12 (2018) 2048–2055.
[14] X. Dai, N. Sun, S.O. Nielsen, B.B. Stogin, J. Wang, S. Yang, T.S. Wong, Sci. Adv. 4 (2018) q919.
[15] F. Zhang, P. Ju, M. Pan, D. Zhang, Y. Huang, G. Li, X. Li, Corros. Sci. 144 (2019) 74–88.
[16] H. Zhao, Q. Sun, X. Deng, J. Cui,Adv. Mater. 30 (2018), 1802141.
[17] P. Wang, T. Li, D. Zhang, Corros. Sci. 128 (2017) 110–119.
[18] M. Tenjimbayashi, S. Nishioka, Y. Kobayashi, K. Kawase, J. Li, J. Abe, S. Shiratori, Langmuir 34 (2018) 1386–1393.
[19] H. Luo, S. Yin, S. Huang, F. Chen, Q. Tang, X. Li, Appl. Surf. Sci. 470 (2019) 1139–1147.
[20] P. Wang, D. Zhang, S. Sun, T. Li, Y. Sun, ACS Appl. Mater. Interface 9 (2016) 972–982.
[21] P. Wang, Z. Lu, D. Zhang, Corros. Sci. 93 (2015) 159–166.
[22] C.S. Ware, T. Smith-Palmer, S. Peppou-Chapman, L.R.J. Scarratt, E.M. Humphries, D. Balzer, C. Neto, ACS Appl. Mater. Interface 10 (2018) 4173–4182.
[23] L. Xiao, J. Li, S. Mieszkin, F.A. Di, A.S. Clare, ACS Appl. Mater. Interface 5 (2013) 10074–10080.
[24] J. Zhang, C. Gu, J. Tu, ACS Appl. Mater. Interface 9 (2017) 11247–11257.
[25] Y. Tuo, H. Zhang, W. Chen, X. Liu, Appl. Surf. Sci. 423 (2017) 365–374.
[26] T. Xiang, M. Zhang, H.R. Sadig, Z. Li, M. Zhang, C. Dong, L. Yang, W. Chan, C. Li, Chem. Eng. J. 345 (2018) 147–155.
[27] D. Jiang, X. Xia, J. Hou, G. Cai, X. Zhang, Z. Dong, Chem. Eng. J. 373 (2019) 285–297.
[28] T. Xiang, S. Zheng, M. Zhang, H.R. Sadig, C. Li, ACS Sustain. Chem. Eng. 6 (2018) 10960–10968.
[29] P. Wang, Z. Lu, D. Zhang, Corros. Sci. 93 (2015) 159–166.
[30] C.S. Ware, T. Smith-Palmer, S. Peppou-Chapman, L.R.J. Scarratt, E.M. Humphries, D. Balzer, C. Neto, ACS Appl. Mater. Interface 10 (2018) 4173–4182.
[31] A.K. Epstein, T.S. Wong, R.A. Belisle, E.M. Boggs, J. Aizenberg, Proc. Natl. Acad. Sci. U. S. A. 109 (2012) 13182.
[32] M. Fu, M. Hultmark, Lubricant Retention for Liquid Infused Surfaces Exposed to Turbulent Flow, APS Meeting, Boston, Massachusetts, 2015.
[33] S. Rowthu, P. Hoffmann, ACS Appl. Mater. Interface 10 (2018) 10560–10570.
[34] H. Qian, D. Xu, C. Du, D. Zhang, X. Li, L. Huang, L. Deng, Y. Tu, A.J.M.C. Mol, H. Terryn, J. Mater. Chem. A 5 (2017) 2355–2364.
[35] D.J. Donahue, F.E. Bartell, J. Phys. Chem. 56 (1952) 480–489.
[36] S. Sett, X. Yan, G. Barac, L.W. Bolton, N. Miljkovic, ACS Appl. Mater. Interface 9 (2017) 36400–36408.
[37] R. Jeltes, W.A.M.D. Tonkelaar, Water Res. 6 (1972) 271–278.
[38] C. Howell, T.L. Vu, C.P. Johnson, X. Hou, O. Ahanotu, J. Alvarenga, D.C. Leslie, O. Uzun, A. Waterhouse, P. Kim,Chem. Mater. 27 (2016), 557762294.
[39] A. Vorobev, Curr. Opin. Colloid Interface 19 (2014) 300–308.
[40] Y. Cheng, H. Suhonen, L. Helfen, J. Li, F. Xu, M. Grunze, P.A. Levkin, T. Baumbach, Soft Matter 10 (2014) 2982–2990.
[41] K. Rykaczewski, T. Landin, M.L. Walker, J.H.J. Scott, K.K. Varanasi, ACS Nano 6 (2012) 9326–9334.
[42] S. Anand, A.T. Paxson, R. Dhiman, J.D. Smith, K.K. Varanasi, ACS Nano 6 (2012) 10122–10129.
[43] D.J. Preston, Y. Song, Z. Lu, D.S. Antao, E.N. Wang, ACS Appl. Mater. Interface 9 (2017) 42383–42392.
[44] J.D. Smith, R. Dhiman, S. Anand, E. Rezagarduno, R.E. Cohen, G.H. Mckinley, K.K. Varanasi, Soft Matter 9 (2013) 1772–1780.
[45] D. Wu, D. Zhang, Y. Ye, L. Ma, B. Minhas, B. Liu, H.A. Terryn, J.M.C. Mol, X. Li, Chem. Eng. J. 368 (2019) 138–147.
[46] S.K. Rawal, A.K. Chawla, R. Jayaganthan, R. Chandra, J. Mater. Sci. Technol. 28 (2012) 512–523.
[47] D.R. Thompson, E. Kougoulos, A.G. Jones, M.W. Wood-Kaczmar, J. Cryst. Growth 276 (2005) 230–236.
[48] D. Zhang, H. Qian, L. Wang, X. Li, Corros. Sci. 103 (2016) 230–241.
[49] S. Wang, H. Peng, Z. Shao, Q. Zhao, N. Du, Surf. Coat. Technol. 286 (2016) 155–164.
[50] M.M. Ali, V. Raj, J. Mater. Sci. Technol. 29 (2013) 595–602.
[51] Y. Zuo, R. Pang, W. Li, J.P. Xiong, Y.M. Tang, Corros. Sci. 50 (2008) 3322–3328.
[52] N. Hu, X. Dong, X. He, J.F. Browning, D.W. Schaefer, Corros. Sci. 97 (2015) 17–24.
[53] V. Moutarlier, M.P. Gigandet, B. Normand, J. Pagetti, Corros. Sci. 47 (2005) 937–951.
[54] M. García-Rubio, P. Ocón, M. Curioni, G.E. Thompson, P. Skeldon, A. Lavía, I. García, Corros. Sci. 52 (2010) 2219–2227.
[55] J. Hitzig, K. Jüttner, W.J. Lorenz, W. Paatsch, Corros. Sci. 24 (1984) 945–952.
[56] M.E. Orazem, B. Tribollet, V. Vivier, D.P. Riemer, E. White, A. Bunge, J. Braz. Chem. Soc. 25 (2014) 532–539.
[57] B. Hirschorn, M.E. Orazem, B. Tribollet, V. Vivier, I. Frateur, M. Musiani, Electrochim. Acta 55 (2010) 6218–6227.
[58] J.J. Suay, E. Gimenez, T. Rodrıguez, K. Habbib, J.J. Saura, Corros. Sci. 45 (2003) 611–624.
[59] V.R. Capelossi, M. Poelman, I. Recloux, R.P.B. Hernandez, H.G. de Melo, M.G. Olivier, Electrochim. Acta 124 (2014) 69–79.
[60] N.D. Nam, J.G. Kim, Y.J. Lee, Y.K. Son, Corros. Sci. 51 (2009) 3007–3013.
[61] L.B. Boinovich, A.M. Emelyanenko, A.D. Modestov, A.G. Domantovsky, A.A. Shiryaev, K.A. Emelyanenko, O.V. Dvoretskaya, A.A. Ganne, Corros. Sci. 112 (2016) 517–527.
[62] U. Trdan, T. Sano, D. Klobčar, Y. Sano, J. Grum, R. Šturm, Corros. Sci. 143 (2018) 46–55.